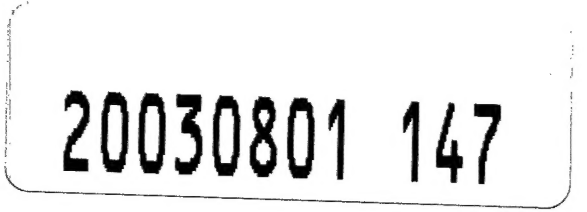


REPORT DOCUMENTATION PAGE

*Form Approved
OMB No. 0704-0188*

Public reporting burden for this collection of information is estimated to average 1 hour per response, including the time for reviewing instructions, searching existing data sources, gathering and maintaining the data needed, and completing and reviewing this collection of information. Send comments regarding this burden estimate or any other aspect of this collection of information, including suggestions for reducing this burden to Department of Defense, Washington Headquarters Services, Directorate for Information Operations and Reports (0704-0188), 1215 Jefferson Davis Highway, Suite 1204, Arlington, VA 22202-4302. Respondents should be aware that notwithstanding any other provision of law, no person shall be subject to any penalty for failing to comply with a collection of information if it does not display a currently valid OMB control number. **PLEASE DO NOT RETURN YOUR FORM TO THE ABOVE ADDRESS.**

1. REPORT DATE (DD-MM-YYYY) 19 May 2003		2. REPORT TYPE Technical Paper		3. DATES COVERED (From - To)	
4. TITLE AND SUBTITLE A Torsional Balance for the Characterization of MicroNewton Thrusters				5a. CONTRACT NUMBER F04611-99-C-0025	5b. GRANT NUMBER
				5c. PROGRAM ELEMENT NUMBER	
6. AUTHOR(S) Manuel Gamero-Castano				5d. PROJECT NUMBER 1011	5e. TASK NUMBER 001V
				5f. WORK UNIT NUMBER	
7. PERFORMING ORGANIZATION NAME(S) AND ADDRESS(ES) Busek Co. Inc. 11 Tech Circle Natick, MA 01760				8. PERFORMING ORGANIZATION REPORT NUMBER	
9. SPONSORING / MONITORING AGENCY NAME(S) AND ADDRESS(ES) Air Force Research Laboratory (AFMC) AFRL/PRS 5 Pollux Drive Edwards AFB CA 93524-7048				10. SPONSOR/MONITOR'S ACRONYM(S)	
				11. SPONSOR/MONITOR'S NUMBER(S) AFRL-PR-ED-TP-2003-135	
12. DISTRIBUTION / AVAILABILITY STATEMENT Approved for public release; distribution unlimited.					
13. SUPPLEMENTARY NOTES					
14. ABSTRACT					
					
15. SUBJECT TERMS					
16. SECURITY CLASSIFICATION OF: a. REPORT Unclassified			17. LIMITATION OF ABSTRACT b. ABSTRACT Unclassified	18. NUMBER OF PAGES c. THIS PAGE Unclassified	19a. NAME OF RESPONSIBLE PERSON Sheila Benner
					19b. TELEPHONE NUMBER (include area code) (661) 275-5693

FILE

MEMORANDUM FOR PRS (Contractor Publication)

FROM: PROI (STINFO)

19 May 2003

SUBJECT: Authorization for Release of Technical Information, Control Number: AFRL-PR-ED-TP-2003-135
Manuel Gamero-Castano (Busek), "A Torsional Balance for the Characterization of MicroNewton Thrusters"

Bromaghin

Journal - "Review of Scientific Instruments"
(Deadline = N/A)

(Statement A)

A Torsional Balance for the Characterization of MicroNewton Thrusters

Manuel Gamero-Castaño

Busek Co. Inc., 11 Tech Circle, Natick, Massachusetts 01760

Prepared for submission to Review of Scientific Instruments

Abstract

We describe the performance of a torsional balance suitable for the study of microNewton thrusters. A design based on flexural pivots and electrostatic forces (for calibration and active damping) makes it possible to test thrusters with a mass of a few kilograms, and measure sub-microNewton level forces with high accuracy and a resolution better than $0.03 \mu\text{N}$. The usefulness of the balance is proved by measuring the performance of two different electric propulsion accelerators: a colloid thruster generating thrust in the 2 to $15 \mu\text{N}$ range, and a micro pulsed plasma thruster yielding single impulse bits of $19 \mu\text{Ns}$. The low noise figure of the balance (below $0.1 \mu\text{N}/\sqrt{\text{Hz}}$ in the 7 mHz to 1 Hz bandwidth) will make it possible to measure the thrust noise requirements imposed in colloid thrusters by missions such as the Space Technology 7 and the Laser Interferometer Space Antenna.

Approved for public release; distribution unlimited.

I. Introduction.

In addition to the expected proliferation of nano and micro satellites, ongoing scientific missions, such as NASA's Space Technology 7 (ST7),¹ and NASA and ESA's Laser Interferometer Space Antenna (LISA)² need propulsion at the microNewton level to achieve their mission goals. The propulsion requirements can be stringent. For example, the NASA ST7 mission calls for thrusters capable of delivering thrust along the 2 to 20 μN range, with a resolution of 0.1 μN , and a noise figure better than $0.1 \mu\text{N}/\sqrt{\text{Hz}}$ in the 1 mHz to 100 mHz bandwidth. Furthermore, the thrusters must operate continuously.

Devices of the type of micro pulsed plasma thrusters (microPPT)³ and solid propellant micro thrusters⁴ are being developed to fill this propulsion niche. Field emission electric propulsion (FEEP)⁵ and colloid thrusters⁶ are generally recognized as the two existing technologies that can match the exceptional requirements imposed by missions like ST7 or LISA. The development of these technologies depends on the characterization of their propulsive properties; in particular, measuring the thrust with the required precision is paramount. Although diagnostic tools such as the time of flight technique can be used to measure thrust in some cases, it is apparent that a force balance, or thrust stand, is a more universal and direct solution, and hence the preferred apparatus.

Several thrust stand designs able to resolve forces at the microNewton level appear in the literature.^{4,7,8} The work by Ziemer deserves special mention because of its quality and characterization of different thrusters.⁹ A variety of technical hurdles handicaps the design and operation of microNewton thrust stands: the weight of the thruster can be as large as a few kilograms, and matching structural strength and

measuring sensitivity is difficult; the inherently "noisy" environment surrounding the balance can completely overwhelm its motion; accurate calibration at this low force level is an additional problem; and, in some cases, the natural dynamics of the balance have to be compensated to obtain a more tractable response.

We present in this paper a torsional balance specially designed to test micro propulsion thrusters. It can support weights of up to 44 kg, and measure forces with a resolution better than $0.03 \mu\text{N}$. Its accuracy is limited only by the precision with which linear distances and voltages can be measured. The article is organized as follows: after this introductory section we will describe the main features of the torsional balance. Section III presents measurements of the 'continuous' thrust produced by a colloid thruster. The capability of the balance for measuring impulse bits is exemplified in section IV using a microPPT. The article then ends with some brief conclusions. All the results presented in this article were taken under actual experimental conditions, which included work in vacuum (provided by a 250 l/s turbomolecular pump and a 13.8 cfm belt-drive mechanical pump) while supporting a thruster (typically 0.5 kg) and a counterweight.

II. Balance description.

Figure 1 shows a schematic of the torsional balance. An aluminum frame fixed to the vacuum facility supports the swinging arm. The inclination of the frame is adjusted with two stepper motors. The arm rotates around the axis defined by two aligned flexural pivots (Lucas Aerospace, Utica, NY 13503) attached to both the frame and the arm. Each pivot can support an axial load of up to 431 N. The linear displacement of the arm at

0.220 m from the axis of rotation is measured with a fiber optic displacement sensor, LDS (Philtec, Arnold, MD 21012). Its nominal resolution is 5.0 nm in the DC-100 Hz range, dropping to 0.15 μ m at a frequency of 200 kHz. The relation between the output of the sensor (the signal in Volts reported in some of the following figures) and the optical gap was calibrated in situ with a 10 μ m resolution micrometer. Typically, the nominal value of the gap was 0.1 mm, well within the range of linear operation of the sensor. Its calibration value is 8.03 μ m/V.

A set of cylindrical electrodes was used to calibrate the balance displacement resulting from a given torque. The electrode attached to the balance had a diameter of 5.08 cm, while the one attached to the external micrometer had a diameter of 1.90 cm; the gap between them, L , was typically 1.10 mm (the actual value was measured for each calibration). The distance between the center of the electrodes and the axis of the balance was 0.266 m. An electrostatic force is a good option to excite the balance because: a) it acts at a distance, i.e. there is no physical contact between the rotating arm and the forcing element; b) the electrostatic force can be accurately computed; c) its amplitude can be varied "continuously", and d) its time variation can be controlled in scales much smaller than that of the characteristic response time of the balance. The electrostatic force, F , on the surface of the electrodes was computed using the software packages Maxwell 2D and Maxwell 3D, versions 9 (the 2D and 3D calculations converged within 0.5%). The calculated values are well fitted by the formula:

$$\frac{F}{V^2} = 1.262 \times 10^{-9} \frac{1}{L^2} (1 + 138.1xL), \quad \text{in } \mu\text{N/V}^2, L \text{ expressed in meters} \quad (1)$$

where V is the voltage difference between the electrodes. Note that, for a 1 mm gap, the calculated force is 13.8% larger than the estimate derived from the assumption of a

homogeneous electric field between the electrodes. The difference is due to the excess charge on the edges existing in the real electrode geometry, which is accurately captured by the Laplace's equation solver. We have used the calibration in (1) to compute all the force measurements in this article. We also used electrostatic forces, driven by an analog circuit controller, to implement an active linear damper and reduce the oscillatory nature of the balance's motion.

The dynamics of the torsional balance are well described by the harmonic oscillator equation:

$$\ddot{\vartheta} + \frac{\lambda}{I} \dot{\vartheta} + \frac{\kappa}{I} \vartheta = \frac{1}{I} L(t) \quad (2)$$

where ϑ is the rotation angle of the arm, I is its moment of inertia about the axis of rotation, and λ and κ are damping and torsional spring rate constants. $L(t)$ is the torque applied to the balance, which can be a function of time. Figure 2 illustrates how the balance responds to a torque applied with the calibration electrodes. A step force of 4.11 μN (torque of 1.09 μNm) is exerted and the resulting motion of the balance is monitored. Note that the noise to signal ratio of the balance output is quite small at this microNewton measurement level. Repeating this measurement with different excitation levels, a static calibration of the balance is computed. Such a calibration is shown in figure 3, where all four axes are used to display the relevant parameters (calibration force and torque, LDS output in Volts, and displacement measured by the LDS). The relation between the LDS output and the exciting torque is quite linear and has a negligible interception with the y-axis, which makes it possible to compute the torsional spring rate accurately. We get $\kappa = 0.0192 \mu\text{N/mV}$, or written in the physical units of equation (2), $\kappa = 0.140 \text{ Nm/rad} = 0.00244 \text{ Nm/degree}$ (the relation between LDS output and displacement is $8.03 \mu\text{m/V}$;

the distance between LDS and the axis of rotation is 0.220 m; the lever arm of the calibration electrode is 0.266 m).

The magnitude of the sinusoidal transfer function of the balance, $\|G(f)\|$, is shown in figure 4. The frequency response was obtained with a colloid thruster weighing 0.450 kg and an identical counterweight placed on the balance, which increased its moment of inertia and hence its natural period. A sinusoidal torque at varying frequencies was applied with the calibration electrodes. The transfer function in figure 4 is the product of the transfer functions of the second order system associated with the balance dynamics, and that of an analog, first order RC filter used to condition the output of the LDS. The resulting response resembles a low pass filter with a cut off frequency around 0.4 Hz. The natural frequency of the balance can be estimated from the resonance peak in figure 4, $f_n \sim 0.25$ Hz.

III. Measuring “continuous” thrust: colloid thrusters.

Colloid thrusters are electrostatic accelerators of charged electrospray droplets.^{6,10} They generate thrust continuously in the microNewton range, with a low noise spectrum and ample throatability. These capabilities are essential for drag-free missions such as the New Millennium Program’s ST7, which is designed to maintain a spacecraft’s position with respect to a free-floating test mass to less than $10 \text{ nm}/\sqrt{\text{Hz}}$, over the frequency range 1 mHz to 30 mHz.¹¹ In fact, colloid thrusters are one of the two new technologies, gravity sensors being the second one, on which the ST7 mission is based. We have used the torsional balance to measure the thrust generated by a 6-emitter colloid thruster. The electrospray source was mounted inside a grounded aluminum box, which

also contained a reservoir filled with propellant (see figure 1 for a sketch of the thruster). The lever arm of the thruster was 0.254 m. A typical measurement session is illustrated in figure 5. We plot the signals associated with the emitter voltage, V_n , the electrospray beam current, I_n , and the balance output, T , as a function of time. The measuring procedure is as follows: the electrospray source is initially in operation ($V_n = 2.07$ kV, $I_n = 2.75$ μ A), yielding a thrust of 9.10 μ N. The offset of the balance signal is determined by turning off the power connected to the electrospray source (see voltage and current curves at $t \sim 46$ s), which causes the balance signal to relax to its equilibrium position. Once the equilibrium position is determined, the electrospray source is turned back on. It takes a few second for the thrust to reach its steady state value because the extra amount of propellant surrounding the emitters, accumulated during the power off period, needs to be fully extracted. The acceleration voltage is then ramped up, which results in an increase of the thrust, until a value of 5.07 kV (14.90 μ N) is reached. The equilibrium position of the balance is determined again by shutting down the electrospray source, and finally the acceleration voltage is ramped down to the initial value of 2.07 kV. This experimental run was taken at constant propellant mass flow rate (i.e., roughly constant beam current). We have repeated this procedure at different flow rates and mapped the thrust versus beam current versus acceleration voltage surface in the 2.40 to 14.90 μ N, 1.34 to 2.75 μ A, and 2.07 to 5.07 kV domain.¹²

After demonstrating throatability and quasi continuous thrust variation, we will analyze the power spectrum of the balance output. We aim to find the lower limit beyond which the noise of the colloid thruster cannot be directly characterized by the balance (the noise figure is the most stringent requirement imposed on the thruster performance by

missions like ST7). Figure 6 shows a recording of the balance output during 10,000 s at a sampling rate of 0.2 seconds. Both calibration electrodes and colloid thruster are off; i.e., this spectrum reflects the free motion of the balance in the absence of intentionally applied torques. The thrust scale is referred to the position of the colloid thruster (lever arm of 0.254 m). An interesting feature of these data is the small variation of the balance offset, especially in the interval between 5,000 and 10,000 seconds. We can estimate the balance resolution by computing the standard deviation of these data. To do so, we divided the data into 20-second windows (this stretch, made of five natural periods of the balance-colloid thruster system, contains enough points to obtain a representative average of the balance output), computed the standard deviation of each window, and averaged the standard deviations. We obtain an averaged standard deviation of $0.034 \mu\text{N}$. Note that this is a conservative estimate for the resolution, because at this 20-second scale most of the signal variation is actually due to oscillations of the balance at frequency values around 0.25 Hz (the energy transmitted to the balance by spurious sources of external noise is mostly dissipated by oscillations at the balance's natural frequency), and the effect of these oscillations on the measurement is greatly reduced by averaging the signal during five natural periods of the balance. A second relevant figure of the balance performance is its offset drift rate. The average of the values for each 20-second window is 0.80 nN/s , and thus the averaged drift of the balance during a 20 s period is $0.016 \mu\text{N}$.

The noise spectrum of the 10,000 seconds series, figure 6, is shown in figure 7. The time span of this series makes it possible to compute the power spectrum down to the low frequencies of interest for the ST7 mission. We have used the following standard

procedures to compute the spectrum: it is based on the power spectrum density per unit time of the thrust; in order to reduce the variance of the periodogram estimation, the original series of sampled points was partitioned into 10 segments, and we averaged the square root of the power spectra at every discrete frequency; and the linear trend was subtracted from each data window. Returning to figure 7, note that the noise spectrum of the balance is approximately $0.02 \mu\text{N}/\sqrt{\text{Hz}}$ at 0.1 Hz, and monotonically increases for lower frequencies, reaching the value of $0.1 \mu\text{N}/\sqrt{\text{Hz}}$ at 7 mHz. We expect to improve this figure by reducing external noise sources, and thus positively test the $0.1 \mu\text{N}/\sqrt{\text{Hz}}$ constraint imposed by the ST7 mission on colloid thrusters along the required bandwidth, [1 mHz, 100 mHz]. Spectrum in the figure 7 also shows how the noise peaks around the natural frequency of the balance, $f_n \sim 0.25$ Hz. The noise increase at still larger frequencies is irrelevant to our application, and it is likely due to poor filtering of electrical noise typical of higher frequencies, which is aliased into the bandwidth of figure 7. The aliasing is amplified above 0.25 Hz by the steep decline of the balance's transfer function (see figure 4).

IV. Thrust impulse bit measurement: micro pulsed plasma thruster.

The total momentum generated by a pulsed plasma thruster can be accurately measured with a torsional balance. This thruster operates through brief plasma discharges (typically they last a few microseconds), each of them transferring a given momentum, or thrust impulse bit, and which repeated at a given frequency translate into an averaged thrust. Because, during each shot, the interaction forces between the exhaust plasma and the thruster occur in an instant, t_d , several orders of magnitude smaller than

the natural period of the balance, t_n , the motion of the latter cannot follow instantaneously the exciting force. But, because the momentum is conserved, the impulse bit associated with the discharge can be accurately modeled by an initial condition on the balance velocity. Thus, the response of the balance to an impulsive force is described by equation (2) with the right-hand side equal to zero, and with initial conditions $\vartheta(0) = 0$ and $\dot{\vartheta}(0) = P/I$, where P is the time integral of the impulsive force (or, more correctly, the impulsive torque) associated with the discharge:

$$P = \int_0^{t_d} L(t) dt, \quad t_d \ll t_n \quad (3)$$

Thus, as long as the characteristic time of the discharge is much smaller than the characteristic response time of the balance, the motion of the balance, $\vartheta(t)$, is strictly a function of the total momentum transferred by the discharge, P , and does not depend on the particular shape of $L(t)$. Using this fact, together with our electrostatic calibration forces, we will show in the following paragraphs how to obtain an accurate calibration between thrust impulse bit and the balance signal. In these experiments the balance was holding a microPPT¹³ weighing 0.652 kg and an identical counterweight in the opposite side; the lever arm of the microPPT was 0.174 m; and the lever arm of the calibration electrode was, as in the colloid thruster experiments, 0.266 m.

First, it is easy to prove that the solution for $\vartheta(t)$ is proportional to P , and in particular, the height of the first oscillation peak resulting from the impulsive excitation is also proportional to P . Second, because $\vartheta(t)$ is independent of the exact shape of $L(t)$ for a given P , we can use the "arbitrarily fast acting" electrostatic force to obtain the desired calibration. The methodology is illustrated in figures 8, 9 and 10. Figure 8 plots the voltage difference between the electrodes while simulating an impulsive force. The

interaction lasted 40 ms, 100 times shorter than the natural period of the balance; it has a pulse-like shape topping 677 V, and the associated momentum is 17.8 μ Ns (or 4.73 μ Nms). The motion of the balance caused by this pulse is shown in figure 9. Note that the electrostatic damper eliminated the oscillations after a few cycles. The height of the first peak, h , as given by the electronics of the LDS, is 1.07 V. This process can be repeated several times, resulting in the P versus h calibration shown in figure 10, which collects impulse bit values in the range 3.45 μ Ns to 39.3 μ Ns, with excitation intervals between 20 ms and 80 ms. The calibration exhibits a very good linearity and a small interception of the linear fitting with the ordinate axis.

Figure 11 shows the response of the balance to a single shot of the microPPT. The signal named ‘discharge voltage’ was a mere indication of when the microPPT is triggered. Naturally, the evolution of the signal is similar to that shown in figure 9, since the impulsive nature of the excitation was the same in both cases. The height of the first oscillation peak is 0.769 V, and hence the total momentum associated with the discharge is 19.4 μ Ns (the lever arm of the μ PPT is 0.174 m; the lever arm of the calibration electrodes is 0.266 m). The discharge voltage was 1460 V, and the energy stored in the capacitors previous to the discharge was 2.1 J. Finally, figure 12 shows the impulse bits of 20 single shots, all of them having the discharge parameters of the previous case. The balance measurements indicate that the microPPT discharges are quite repeatable, at least from the point of view of momentum transfer to the thruster.

V. Conclusion.

We have described a torsional balance well suited for the characterization of microNewton thrusters. Although it was initially designed to study the 'continuous' thrust of colloid thrusters, we have demonstrated that it can accurately measure the impulse bits typical of a microPPT as well.

A main novelty of this work is the use of electrostatic forces to calibrate the balance for both 'continuous' and 'impulsive' measurements. The accuracy and resolution of the measuring techniques described in this article are guaranteed by the arbitrary accuracy and resolution with which the parameters (mainly distances and voltage values) entering in the calibrations can be determined. The high linearity of the calibrations shown in figures 3 and 10 are indicative of the quality of these measurements.

In its current development state, this torsional balance has let us confirm positively that the noise spectrum of colloid thrusters in the bandwidth 7 mHz to 100 mHz is below the constraint ($0.1 \mu\text{N}/\sqrt{\text{Hz}}$) imposed by the ST7 mission.^{1,12} Although we still need to improve the experimental conditions in order to prove this noise figure down to 1 mHz, it should be pointed out that these results represent the current state of the art of high precision micro propulsion.

Acknowledgments.

The construction of the torsional balance was funded by a NASA SBIR contract. Additional research work was funded by the Jet Propulsion Lab and the U.S. Air Force Research Laboratory. We greatly acknowledge the support given by the technical

monitors of these programs, J. Sovey (NASA), W. Folkner and G. Man (JPL), and D. Bromaghim (AFRL).

We also acknowledge the help of Prof. M. Martínez-Sánchez (MIT) and V. Hruby (Busek), both of whom are responsible for the original mechanical design of the balance.

Figure captions.

Figure 1. Schematics of the torsional balance.

Figure 2. Balance's response to a $1.09 \mu\text{Nm}$ torque excitation.

Figure 3. Balance's steady state calibration.

Figure 4. Balance's frequency response.

Figure 5. Typical thrust measurements with a colloid thruster.

Figure 6. Recording of the intrinsic motion of the balance during 10,000 s.

Figure 7. Power spectrum density per unit time of the data in figure 6.

Figure 8. Impulsive excitation of the balance using calibration electrodes.

Figure 9. Balance's response to the impulse bit in figure 8.

Figure 10. Impulse bit calibration of the balance.

Figure 11. Balance's motion induced by a single microPPT shot.

Figure 12. Collection of microPPT impulse bits for a nominal set of discharge conditions.

References

¹ Folkner, G. Keiser, S. Buchman, R.L. Byer, V. Hruby, M. Gamero-Castaño Disturbance reduction system: testing technology for precision formation control. Paper 4860-36, Proceeding of SPIE Vol. 4860. SPIE's Astronomical Telescopes and Instrumentation conference, Waikoloa, HI (2002). G. Keiser, S. Buchman, R.L. Byer, M. Folkner, V. Hruby, M. Gamero-Castaño. Disturbance reduction system for testing technology for drag-free operation. Paper 4856-02, Proceeding of SPIE Vol. 4856. SPIE's Astronomical Telescopes and Instrumentation conference, Waikoloa, HI (2002).

² T. T. Hyde, P. G. Maghami. "Precision pointing for the laser interferometry space antenna mission", Paper AAS 03-066, American Astronautical Society Guidance and Control Conference, Breckenridge, CO (2003)

³ M. Martin, P. Klupar, S. Kilberg & J. Winter, "TechSat 21 and Revolutionizing Space Missions Using Microsatellites," Proceeding of the 15th Annual AIAA/USU Conference on Small Satellites, Logan, UT (2001).

⁴ D. White, J. H. Schilling, S. Bushman, G. G. Spanjers, D. R. Bromaghim, J. Lake, M. Dulligan, "AFRL MicroPPT Development for Small Spacecraft Propulsion", Paper AIAA 2002-2120, 33rd Plasmadynamics and Lasers Conference, Maui, HI (2002).

⁵ S. Orieux, C. Rossi & D. Esteve, "Thrust stand for ground tests of solid propellant microthrusters", Review of Scientific Instruments, 73, 2694-2698 (2002).

⁶ S. Marcuccio, A. Genovese & M. Andrenucci, "Experimental Performance of Field Emission Microthrusters", Journal of Propulsion and Power, 14, 1998.

⁷ M. Gamero-Castaño & V. Hruby. "Electrospray as a source of nanoparticles for efficient colloid thrusters", Journal of Propulsion and Power, 17, 977-987 (2001).

⁸ A. J. Jamison, A. D. Ketsdever & E. P. Muntz, "Gas dynamic calibration of a nano-Newton thrust stand", Review of Scientific Instruments, 73, 3629 (2002).

⁹ M. Gamero-Castaño, V. Hruby & M. Martínez-Sánchez "A Torsional Balance that Resolves sub-micro-Newton Forces". Paper IEPC-01-235, 27th International Electric Propulsion Conference, Pasadena, CA (2001).

¹⁰ J. K. Ziemer, "Performance Measurements Using a Sub-Micronewton Resolution Thrust Stand", Paper IEPC-01-238 27th International Electric Propulsion Conference, Pasadena, CA (2001).

¹¹ M. Gamero-Castaño & V. Hruby, "Characterization of a colloid thruster performing in the micro-Newton thrust range". Paper IEPC-01-282, 27th International Electric Propulsion Conference, Pasadena, CA. (2001).

¹² P. G. Maghami, F. L. Markley, M. B. Houghton & C. J. Dennehy, "Design and analysis of the ST7 disturbance reduction system (DRS) spacecraft controller", Paper AAS 03-065, American Astronautical Society Guidance and Control Conference, Breckenridge, CO (2003)

¹³ M. Gamero-Castaño, "Characterization of a six emitter colloid thruster using a torsional balance". In preparation for submission to Journal of Propulsion and Power.

¹⁴ The development of this microPPT is an ongoing collaboration between the U.S. Air Force Research Laboratory and Busek. L. Byrne is responsible for the research work at Busek. D. Bromaghim is the manager of the program at the AFRL.

Figure 1

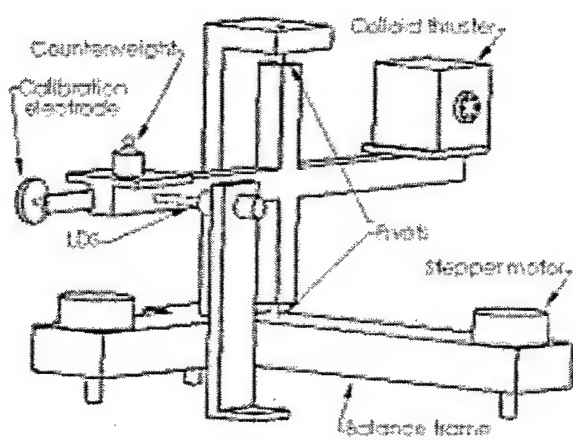


Figure 2

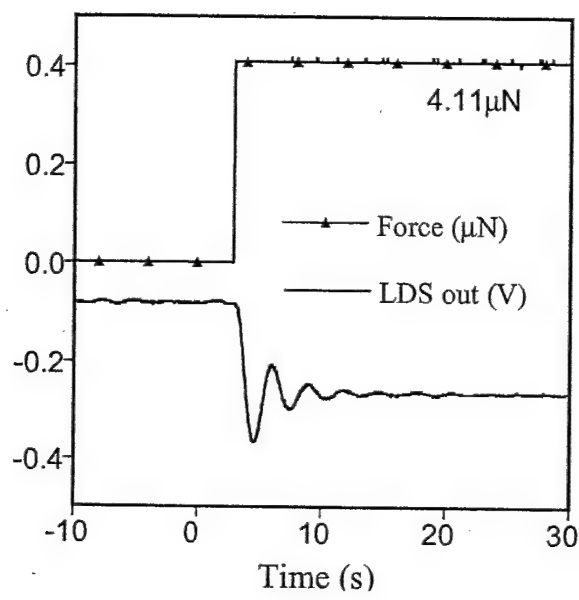


Figure 3

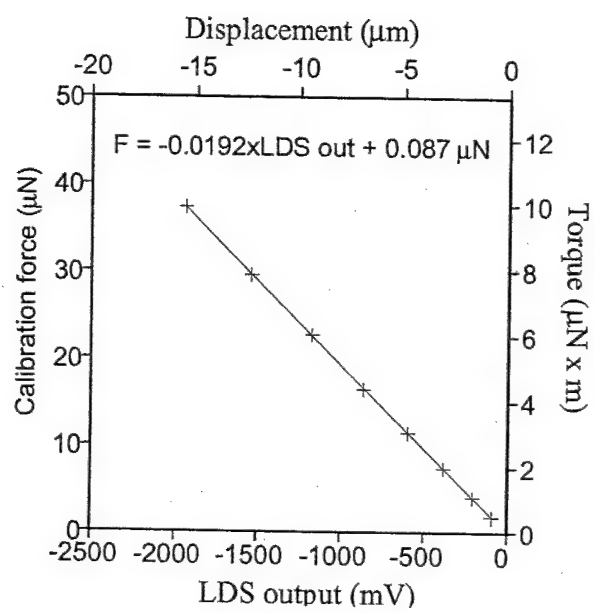


Figure 4

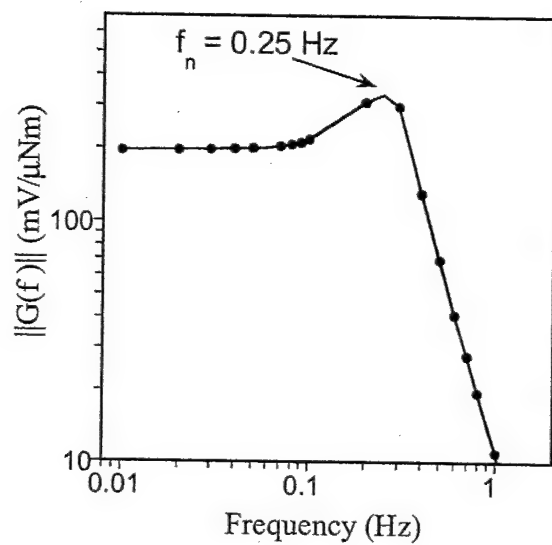


Figure 5

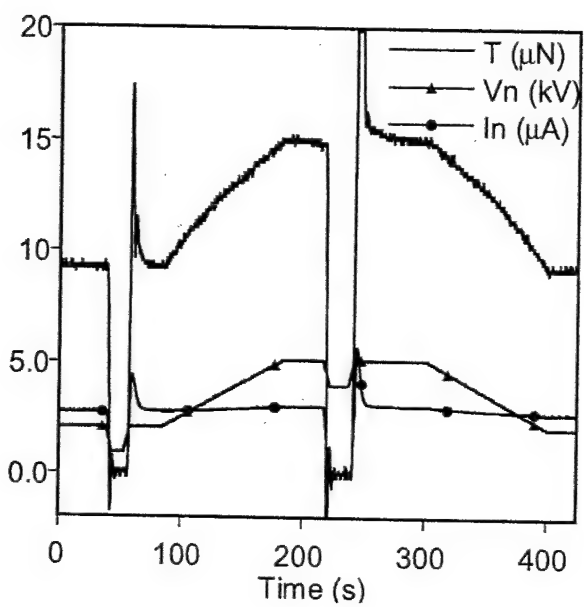


Figure 6

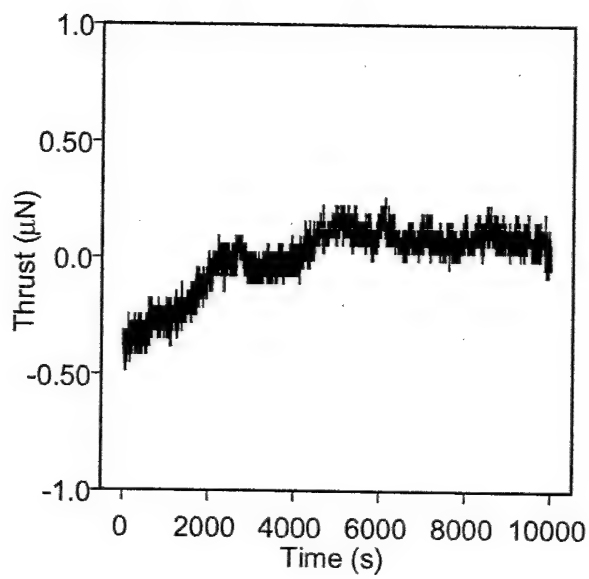


Figure 7

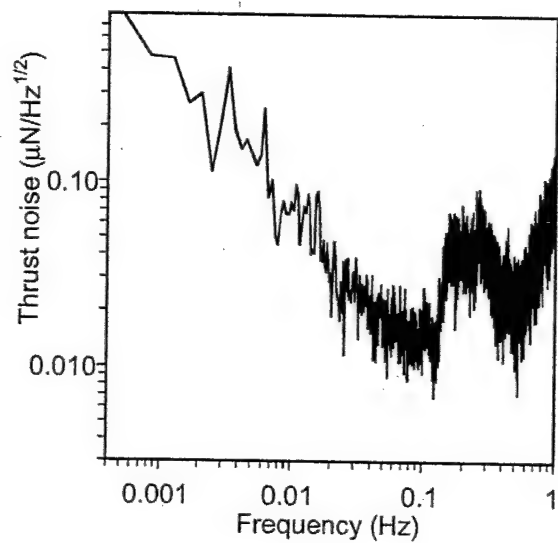


Figure 8

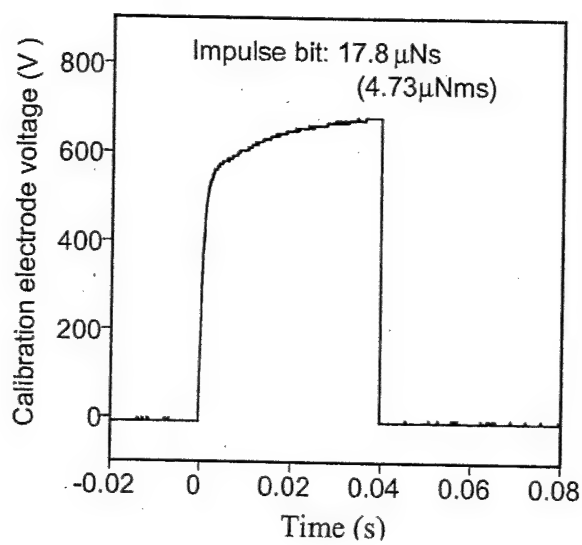


Figure 9

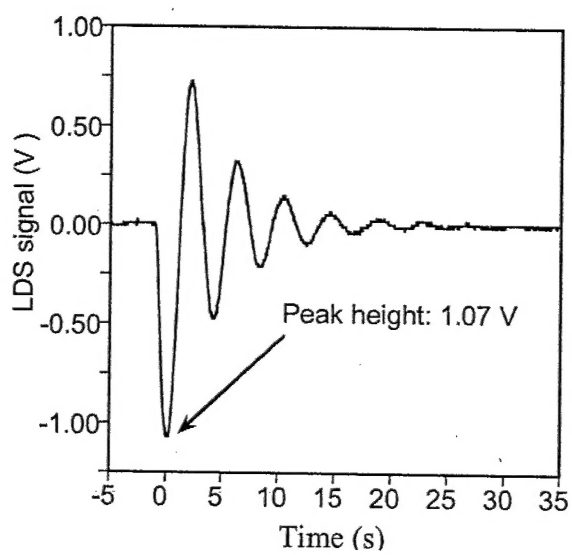


Figure 10

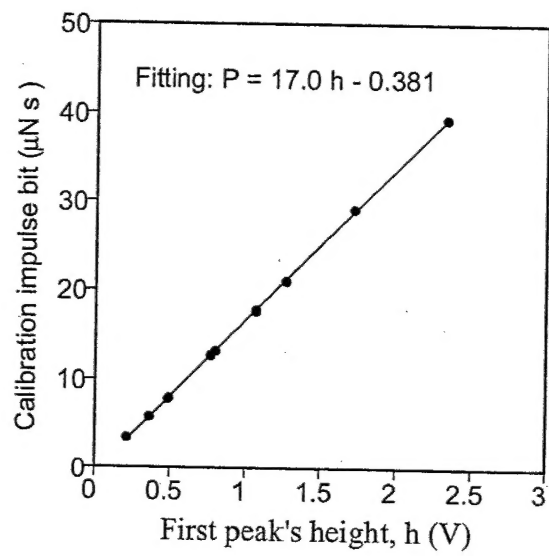


Figure 11

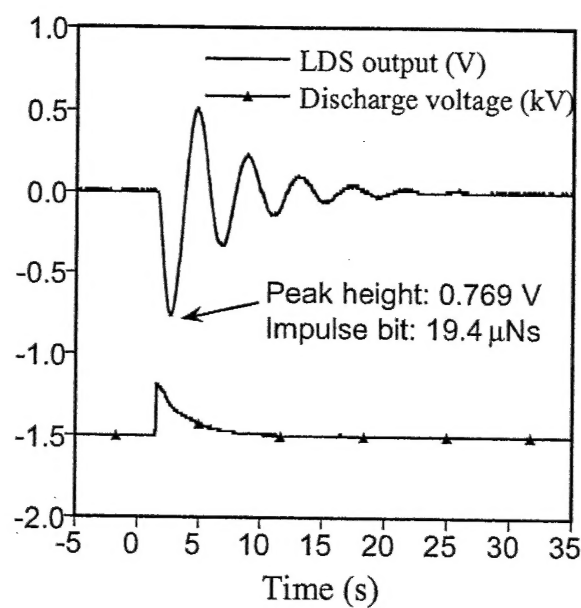


Figure 12

